Calculation of the X-Ray Reflectivity of *b*-Class Mosaic Crystals via the Monte Carlo Method

D. A. Baklanov, I. E. Vnukov, Yu. V. Zhandarmov, G. T. Duong, S. A. Laktionova, and R. A. Shatokhin

Belgorod State University, Belgorod, Russia

Received July 12, 2010

Abstract—*b*-class mosaic crystals, including pyrolytic graphite, are widely used as neutron and X-ray monochromators in experimental physics and ensure a more intense yield of monochromatic radiation than do perfect crystals. A new technique that has been proposed for calculating the X-ray reflectivity of these crystals via the Monte Carlo method is implemented. According to this technique, repeated reflections of photons inside crystals and the experiment geometry can be correctly estimated for an arbitrary mosaicity distribution.

INTRODUCTION

Monochromatic X-ray beams can be produced by diffraction of electromagnetic radiation with continuous and discrete spectra in crystals. The integral reflectivity of mosaic crystals is substantially higher than that of perfect crystals. Crystals can be classified according to degree of perfection on the basis of two criteria: the size of regular blocks or regions and the degree of their mutual disorientation [1]. The first criterion allows division of crystals into *a* and *b* classes. In the *a*-class crystals, separate regions are large enough to stimulate the noticeable influence of primary extinction; i.e., their linear sizes are comparable with primary extinction length l_{ex}. In the *b*-class crystals, the regular block sizes are small. Hence, the effect of primary extinction is hardly observed at all. The second criterion makes it possible to divide crystals into α and β classes. In the α-class crystals, blocks are almost parallel to each other and their mutual disorientation is low. Hence, the contribution of secondary extinction is high. The β-class crystals are characterized by an irregular distribution of blocks. Hence, the contribution of secondary extinction is low.

The X-ray reflectivity of crystals depends on the perfection of their structure. $a\alpha$-class crystals ensure a narrow rocking curve (the full width at half maximum is ~20–30″), and their integral reflectivity is small. $b\beta$-class mosaic crystals exhibit the maximum integral reflectivity. Pyrolytic graphite, which is employed in applied physics to generate quasi-monochromatic X-ray and neutron beams, is a well-known *b*-class mosaic crystal [2, 3].

As was noted in several experimental studies [2], the theory of X-ray diffraction in mosaic crystals [4, 5] sometimes incorrectly describes the results of measurements even in pyrolytic graphite crystals. This is associated, first of all, with the assumptions that mosaic blocks are uniformly distributed across the crystal thickness and their mutual disorientation with respect to the average direction has a Gaussian distribution. The statistical simulation method enables us to ignore these assumptions and estimate all the experimental parameters more correctly: the size and geometry of crystals, the actual mosaicity distribution of samples, multiple reflections inside the crystal, changes in absorption related to the multiplicity of reflections, and so forth.

SIMULATION

Our approach is also based on the theory of X-ray diffraction in mosaic crystals [1, 4, 7] and was partially employed in [6]. The reflectivity of *b*-class mosaic crystals is calculated via the technique implemented for 1D mosaicity distribution and a monodirectional beam of external radiation with a fixed energy. In the general case, a divergent photon beam with a continuous spectrum impinges on or is generated in a crystal. When a monodirectional and monoenergetic photon beam is reflected by the mosaic crystal's element with volume ΔV, we obtain [1]

$$\int P(\theta)\, d\theta = Q\Delta V, \tag{1}$$

where $P(\theta)$ is the reflectivity of the crystalline element at angle θ (its value is proportional to the distribution of mosaic blocks in the crystal [7]) and $Q\Delta V$ is the integral reflectivity from element ΔV. Integral reflectivity Q depends on crystal parameters and radiation energy:

$$Q = \left(\frac{e^2}{mc^2}\right)^2 \frac{N^2\lambda^3}{\sin(2\Theta)} |F_p||F(\mathbf{g})|^2. \tag{2}$$

Here, N is the concentration of scattering centers; λ is the radiation wavelength; Θ is the angle between the

crystal plane and the photon beam direction; and $|F(\mathbf{g})|^2 = |S(\mathbf{g})|^2 \exp(-2W)$, where $|S(\mathbf{g})|^2$ is the structural coefficient, $\exp(-2W)$ is the Debye–Waller coefficient, and $F(\mathbf{g})$ is the Fourier component of the spatial distribution of electrons in a crystal atom ($f(0) = z$, where z is the number of electrons in the atom), and $|F_p|$ is the polarization coefficient related to the polarization of radiation incident on the crystal. If the polarization vector is perpendicular to the diffraction plane, $|F_p| = 1$. In the opposite case, $|F_p| = \cos^2 2\Theta$. If the beam is not polarized, $|F_p| = (1 + \cos^2 2\Theta)/2$.

A reflection process is analyzed by means of the approach proposed in [8] and using several coordinate systems related to the direction of a primary photon beam (the laboratory coordinate system) and the direction of a crystal plane (the crystal coordinate system). Let the photon beam having spectral-angular distribution $N_\gamma(\omega, \mathbf{n})$, where ω is the energy and $\mathbf{n}$ is the unit vector, and directed along the photon momentum propagate in the mosaic crystal with the distribution $P(\mathbf{g})$ of reciprocal lattice vectors. Here, $g = |\mathbf{g}|\boldsymbol{\alpha}$, where $\boldsymbol{\alpha}$ is the unit vector describing the deviation of crystal microblocks from the average direction $\mathbf{g}_0 = \langle \mathbf{g} \rangle$. Vector $\mathbf{g}_0$ is perpendicular to the crystal plane. The angle between this vector and the z axis is $\pi/2 - \Theta_B$. The diffraction plane is defined by vectors $\mathbf{n}$ and $\mathbf{g}$.

In the case of photon diffraction on a microblock (the photon has energy ω and direction $\mathbf{n}$), Bragg's law enables us to define the following requirement to the direction of microblock vector $\mathbf{g}$:

$$\omega = \frac{\mathbf{ng}}{\sqrt{\varepsilon_0}(1 - \mathbf{n'n})} = \frac{|\mathbf{g}|\sin\Theta}{\sqrt{\varepsilon_0}(1 - \cos 2\Theta)}, \tag{3}$$

where $\mathbf{n}'$ is the vector describing the motion direction of the diffracted photon and ε_0 is the medium permittivity. Here and below, the system of units $\hbar = m_e = c = 1$ is used. Hence, an angle between the directions of vectors $\mathbf{n}$ and $\mathbf{g}$ must satisfy the condition

$$\sin\Theta = \frac{|\mathbf{g}|}{2\omega\sqrt{\varepsilon_0}}. \tag{4}$$

In the mosaic crystal, this condition is valid for a set of mosaic blocks governed by the equation

$$\sin\Theta = \frac{(\mathbf{gn})}{|\mathbf{g}|} = \frac{[n_x g_x + n_y g_y + n_z g_z]}{|\mathbf{g}|}. \tag{5}$$

On the basis of this equation, it is possible to determine both mosaic blocks on which this photon can diffract and the motion direction $\mathbf{n}'$ of the diffracted photon. Thus, in the mosaic crystal with thickness Δt, the probability density of reflection of the photon with fixed ω and $\mathbf{n}$ can be expressed as

$$f(\omega, \mathbf{n}) = q(\omega, \mathbf{n})Q(\omega)\Delta t, \tag{6}$$

where $q(\omega, \mathbf{n})$ is the crystal mosaicity coefficient:

$$q(\omega, \mathbf{n}) = \int P_m(\alpha_x(\omega, \mathbf{n}, \alpha_y), \alpha_y) d\alpha_y. \tag{7}$$

Here, $P_m(\alpha_x, \alpha_y)$ is the crystal mosaicity distribution expressed in terms of ω, $\mathbf{n}$,, and α_y ((2)–(5)).

According to the approach developed in [7], for each reflection order i, the diffracted photon yield in the collimator aperture is determined by convolving the spectral-angular distribution of the radiation intensity with the probability density of reflection over all variables, including photon energy, photon emission angles, and crystal thickness. In the crystal layer between diffraction and escape regions, the secondary diffraction of photons reflected in the primary beam direction is calculated similarly. Absorption of photons depends on their free path lengths within the crystal and their energies. This technique makes it possible to determine both the spectral-angular radiation distribution and the realistic mosaicity distribution of a sample. Its main drawbacks are a difficulty of estimating the actual geometry of measurements (crystal rotations, the eventual difference of the mosaicity distribution from a Gaussian form, and so forth), and the uncontrollably varying photon path length in the crystal owing to multiple reflections.

With allowance for (6) and (7), diffraction-induced variations in the number of photons after their passage through the crystal layer with thickness Δt can be expressed as

$$\begin{aligned} \Delta N_\gamma(\omega, \mathbf{n}) &= -N_\gamma q(\omega, \mathbf{n})Q(\omega)\Delta t \\ &= -N_\gamma \mu_{dif}(\omega, \mathbf{n}, \mathbf{g})\Delta t, \end{aligned} \tag{8}$$

where $\mu_{dif}(\omega, \mathbf{n}, \mathbf{g})$ is the linear coefficient of absorption of the radiation with energy ω in motion direction $\mathbf{n}$ owing to diffraction in the mosaic crystal.

According to (8), the dependence between the number of photons and crystal layer thickness t can be written in the conventional form:

$$N_\gamma(\omega, \mathbf{n}, t) = N_0(\omega, \mathbf{n})\exp(-\mu_{tot}t), \tag{9}$$

Here, $N_0(\omega, \mathbf{n})$ is the spectral-angular distribution of radiation incident on the crystal and $\mu_{tot} = \mu_{dif}(\omega, \mathbf{n}, \mathbf{g}) + \mu_{ph}(\omega) + \mu_{inc}(\omega) + \mu_{coh}(\omega) + \mu_{pair}(\omega)$ is the total linear coefficient of absorption of primary radiation. The latter depends on photoabsorption $\mu_{ph}(\omega)$, incoherent (Compton) scattering $\mu_{inc}(\omega)$, coherent scattering $\mu_{coh}(\omega)$, and electron–positron pair generation $\mu_{pair}(\omega)$. Such a notation enables us to describe photon penetration through a mosaic crystal via the well-known statistical simulation method (the Monte Carlo method [9]).

Let us consider the basic stages and approaches of a simulation process by the example of determining the energy resolution and efficiency of crystal-diffraction spectrometers based on mosaic pyrolytic graphite crystals [10]. A bremsstrahlung beam from a disori-

ented tungsten target impinges on the crystal mounted in the goniometer and rotated through the angle $\Theta_B = \Theta_D/2$. Here, Θ_D is the angle of positioning of the detector used to record diffracted radiation. The technique for calculating the spectral-angular distribution of bremsstrahlung, the characteristics of crystals tested, and the layout of experimental equipment are similar to those described in [7].

At energy ω and wave vector $\mathbf{k} = \omega\mathbf{n}\sqrt{\varepsilon_0}$ of the photon, the point of incidence is determined. With allowance for the measured crystal mosaicity distribution, the angle of microblock disorientation with respect to the y axis (α_y) is sought in the crystal coordinate system. Using the values of ω, $\mathbf{k}$, and Θ_B according to (4) and (5), the disorientation angle of the microblock (on which a photon with the given values of ω and $\mathbf{k}$ can diffract) with respect to the x axis (α_x) is found. Next, from the measured mosaicity distribution with respect to the x axis, the probability that such a block exists in the crystal ($w(\alpha_x)$) and the linear coefficient of diffraction absorption of primary photons ($-\mu_{dif} = wQ$) are determined. For the Gaussian distribution of microblocks, the desired probability is expressed as

$$w = \frac{1}{\sqrt{2\pi}\sigma}\exp\left(-\alpha_x^2/2\sigma^2\right), \qquad (10)$$

where σ is the characteristic angle of the mosaicity of the crystal tested.

Thereafter, according to the traditional approach to simulation of photon penetration through a material, the photon path to the interaction point is examined from the expression $l = \ln\xi/\mu_{tot}$, where ξ is a random number from zero to unity, the interaction point coordinates are determined, and the type of a process (diffraction, photoabsorption, or Compton (incoherent) or coherent scattering) is sought. Simulation is performed with the use of the interaction cross sections of low-energy photons described in [11]. To involve the influence of a crystalline structure, correction coefficient $1 - \exp(2W)$ is introduced into the coherent scattering cross section. If the interaction point does not belong to the crystal, photon capture by the detector is verified and a search process is restarted.

Subsequent stages of simulation are determined by the type of interaction. If a photoabsorption process occurs, simulation is repeated. In the case of photon scattering, the energy ω' of the scattered photon and the direction $\mathbf{n}'$ of its motion are determined with the help of the known techniques for simulating photon interaction with a material [9]. Next, microblock disorientation angle α_y is sought, angle α_x is determined, and the photon free path and the type of interaction are sought. If a diffraction process occurs, the law of conservation of momentum enables us to define the wave vector as

$$\mathbf{k} = \mathbf{k}' + \mathbf{g}. \qquad (11)$$

where $\mathbf{k}'$ is the wave vector of the diffracted photon and $\mathbf{g}$ is the vector of the reciprocal lattice of the crystal microblock on which a diffraction process is observed. All three vectors are determined in the laboratory coordinate system. Hence, according to the technique reported in [8], vector $\mathbf{g}$, which is described by microblock disorientation angles α_x and α_y in the crystal coordinate system, must be converted to the laboratory system. Next, on the basis of ω and vectors $\mathbf{g}$ and $\mathbf{n}$, the motion direction of the diffracted photon is defined as

$$\mathbf{n}' = \mathbf{n} - \frac{\mathbf{g}}{\omega\sqrt{\varepsilon_0}}. \qquad (12)$$

At the next stage, for the photon with energy ω and wave vector $\mathbf{k} = \omega\mathbf{n}\sqrt{\varepsilon_0}$, microblock disorientation angle α_y is sought and angles α_x is determined. Next, the free path length is sought, the coordinate of the interaction point is determined, the condition of escape from the crystal is verified, and the condition of interaction is examined. A distinctive feature of the second and subsequent even-order reflections is that a photon is reflected from the opposite side of the plane. Hence, for these reflections, the crystal system is rotated through 180° about the y axis. The history of each photon is traced up to its absorption in the crystal or escape from it and capture by a detector.

The proposed technique has no restrictions on the thickness and geometry of the crystal tested (several samples can be employed), the angular distribution of mosaic blocks, and so forth. The main condition of its applicability is the use of a *b*-class crystal and reliable information on the 2D angular distribution of mosaic blocks in the crystal. In particular, such information can be used to calculate the yield of X-rays emitted at large angles to the primary beam direction when electrons and photons pass through textured polycrystals [12].

Low-energy neutron diffraction is described in the same manner as diffraction of X-rays in mosaic and perfect crystals [13]. According the cited study, integral reflectivity of neutrons from a small element with volume ΔV is $Q_n\Delta V$.. Quantity Q_n can be expressed as

$$Q_n = \frac{\sigma_{Bragg}}{4\pi}\frac{N^2\lambda_n^3}{\sin(2\Theta)}|S(\mathbf{g})|^2\exp(-2W). \qquad (13)$$

Here, λ_n is the de Broglie wavelength and σ_{Bragg} is the elastic neutron scattering cross section in the crystal. Other designations correspond to those employed in previous expressions. Owing to such an analogy, the technique developed for calculating the reflectivity of *b*-class mosaic crystals can be extended to neutron beams, ensuring more accurate determination of neutron absorption in the crystal, increasing the energy range over which the reflectivity can be calculated, and making it possible to exclude a correction coefficient of ≈0.8 used in many investigation for evaluating the contributions of absorption and "residual" elastic scattering [3].

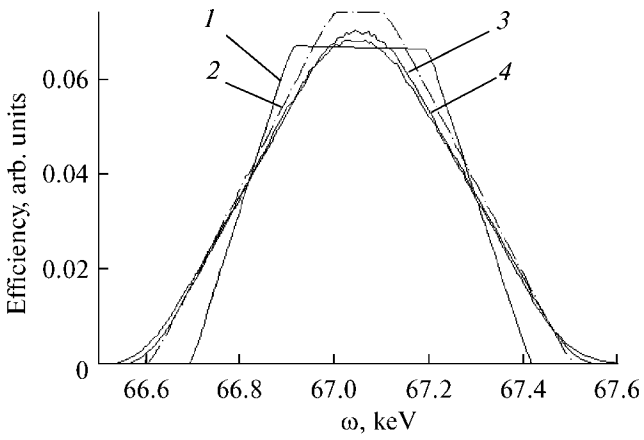

Fig. 1. Calculated efficiencies of the spectrometer at $\Theta_D = 3.16°$ and $\omega \sim 67$ keV.

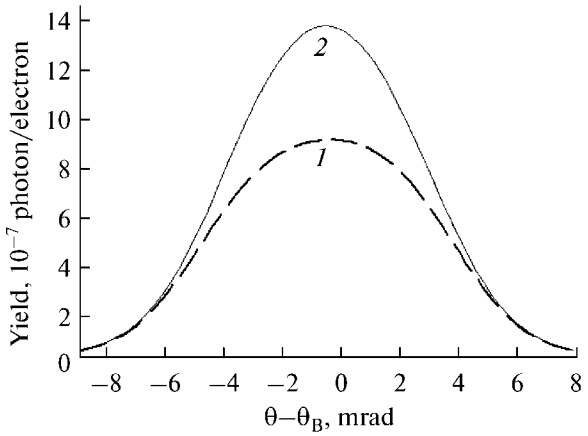

Fig. 2. Orientation dependences of the radiation yield at $\Theta_D = 7.49°$ and $\omega \sim 28.3$ keV.

SIMULATION RESULTS

As was discussed above, the proposed technique for calculating the X-ray reflectivity of *b*-class mosaic crystals has been developed in connection with the necessity of processing search data and investigating the characteristics of parametric X-rays emitted at small angles to the direction of fast electrons moving in a tungsten crystal that were measured in the experiment [10]. Owing to the narrow spectral range of the effect observed, the energy resolution of crystal-diffraction spectrometers employed is of most importance. The calculated absolute radiation yields obtained by means of the proposed technique for determining the characteristics of crystal-diffraction spectrometers under the conditions of the experiment [10] fit the measured results to within an experimental value of 5% or less [14].

In the study cited above, fixed-energy radiation was extracted via two crystal-diffraction spectrometers based on mosaic pyrolytic graphite crystals with sizes of $2.5 \times 6.5 \times 22.5$ and $3.5 \times 5.5 \times 20$ mm, which were mounted in goniometers at distances of 13–15 m from a tungsten crystal employed to produce the X-rays investigated, and NaI(Tl) detectors, each having a size of 40×1 mm, which were placed at distances of 3–5 m from graphite crystals. In the graphite crystals employed, the mosaicity distributions were determined by measuring diffraction curves and identifying diffraction peaks for each of the detector's angular positions in the experiment [7]. In the thinner ($2.5 \times 6.5 \times 22.5$ mm) crystal, such a distribution can be represented as a sum of two Gaussian distributions with the standard deviations σ and S, and $\sigma_m^2 = 9.0 \pm 0.5$ mrad and weighting coefficients $S_1 \approx 0.67 \pm 0.01$ and $S_2 \approx 0.33 \pm 0.05$, 0.05, respectively.

Figure 1 presents the spectrometer efficiencies calculated at a photon energy of first-order reflections of $\omega \approx 67$ keV. Calculations were performed under the following conditions: the collimation angle of reflected radiation in the diffraction plane is $\Delta\Theta_x = 0.42$ mrad, the angular capture in the diffraction plane is $\Delta\theta_x = \pm 0.092$ mrad, and the acceptance is $\Delta\theta_x \Delta\theta_y = 1.84 \times 10^{-7}$ sr. The crystal with sizes of $2.5 \times 6.5 \times 22$ mm was used. The primary spectrum was generated by 500-MeV electrons in the amorphous target 0.5 mm thick.

Dependences *1* and *2* corresponding to a point electron beam were calculated by means of the technique developed in [7]. Curve *1* was obtained by using the angular sizes of a primary radiation beam and the angular capture of the detector of diffracted radiation; i.e., the photon hit coordinate of a crystal analyzer was not taken into account. When photon motion is not directed along the axis of an experimental setup, the detector is positioned at an angle differing from $\Theta_D = 2\Theta_B$ and the shape of the spectral dependence changes (curve *2*). With allowance made for all known experimental parameters (curves *3*, *4*), the simulation results somewhat differ from those obtained according to the technique described in [7]. After introducing the angle of crystal rotation, the point of diffracted photon emission from the crystal, and multiple reflections, the resolution deteriorates to some extent and the reflection efficiency decreases. However, the full width at half maximum remains practically unchanged. Dependence *3*, as well as curves *1* and *2*, was calculated for a point electron beam. Calculations performed with allowance for the spatial distribution of the electron beam impinging on the internal target of a synchrotron [15] (curve *4*) have demonstrated that this parameter weakly affects the spectrometer characteristics.

As can be seen in Fig. 1, the distinction between the dependences calculated via the different approaches is not very significant. The reflectivity increases abruptly with decreasing photon energy. As a consequence, the portion of multiple reflections grows. For example, if the photon energy $\omega = 67$ keV, the portion of quanta that were singly, doubly, and triply reflected in the

crystal was 0.075, 0.004, and 6×10^{-5},, respectively. In the case of $\omega = 28.3$ keV, these values increase up to 0.29, 0.08, and 0.007, respectively. The maximum number of reflections changed from five to six. Since the probability of a portion of multiple reflections grew, the distinction between the distributions obtained via the different approaches became more substantial. At $\omega = 28.3$ keV, the distribution width determined by means of simulation is 20% greater than that calculated via the technique reported in [7].

This effect contributes to the measured characteristics of mosaic crystals and, in a number of cases, can provoke uncontrollable errors. The calculated orientation dependences of the diffracted radiation yield, which were obtained by rotating the graphite crystal at the fixed angle $\Theta_D = 7.49°$ of detector positioning ($\omega =$ 28.3 keV), are depicted in Fig. 2. At the given photon energy, the calculation conditions are identical to those of the experiment [10], except that the crystal mosaicity $\sigma_m = 3$ mrad is used instead of the sum of two Gaussian distributions with different values of σ_m.

Curve *1* c $\sigma = 3.38$ and $\Delta\Theta = 9.37$ mrad) is the result of exact simulation under the conditions of the experiment [10] at the chosen value of σ_m. Here, σ is the standard deviation and $\Delta\Theta$ is the width at half height. Dependence *2* ($\sigma = 3.15$ and $\Delta\Theta = 8.65$ mrad) is obtained by "programmed" elimination of second-order and subsequent reflections. A distinction between σ and σ_m seems to arise because the angular sizes of a radiation beam incident on the crystal and the radiation collimation angle have finite values. As is seen in Fig. 2, multiple reflections substantially deteriorate the observed dependence in comparison with the model curve and the dependence calculated without allowance for subsequent reflections. It differs from the Gaussian, and its width is larger by approximately 10%. Therefore, in the case of crystals with high reflectivities, approximately the same error can arise from measurements of mosaicity distributions and its parameters. This effect plays an important role when mosaic crystals are employed in neutron diffraction processes, because the formula for reflectivity involves the mosaicity distribution width [3]. The approximately similar influence of reflectivity on mosaicity measurements must be observed for $a\alpha$-class mosaic crystals.

CONCLUSIONS

The results of the performed investigations can be summarized as follows.

(i) A new technique for calculating the reflectivity of *b*-class mosaic crystals via the Monte Carlo method has been proposed and implemented. According to this technique, repeated reflections of photons inside crystals and the experiment geometry can be correctly estimated for an arbitrary mosaicity distribution.

(ii) After certain modifications, the proposed technique can be used to calculate neutron reflections from these crystals, making it possible to increase the energy range in which the reflectivity can be calculated and exclude correction coefficients.

(iii) In the investigation of the characteristics of crystals with high reflectivities in the chosen photon energy range, multiple reflections can substantially distort the dependences measured and lead to erroneous measurements of parameters.

ACKNOWLEDGMENTS

We thank our colleagues [6] for participation in the development and implementation of the techniques used in investigations and their assistance in measurements.

This study was supported in part by the Program of Internal Grants of Belgorod State University.

REFERENCES

1. R. W. James, *The Optical Principles of the Diffraction of X-Rays*, revised ed. (Bell, London, 1962; Mir, Moscow, 1966).
2. M. Gambassini, A. Tufanelli, A. Taibi, et al., Med. Phys. **28**, 412 (2001).
3. T. Riste, Nucl. Instrum. Methods Phys. Res **86**, 1 (1970).
4. W. H. Zachariasen, Acta Crystallogr. **23**, 558 (1967).
5. W. H. Zachariasen, *Theory of X-Ray Diffraction in Crystals* (Dover, New York, 1994).
6. M. Chabot, P. Nicolai, K. Wohrer, et al., Nucl. Instrum. Methods Phys. Res. B **61**, 377 (1991).
7. I. E. Vnukov, B. N. Kalinin, G. A. Naumenko, et al., Izv. Vyssh. Uchebn. Zaved., Ser. Fiz., No. 3, 53 (2001).
8. A. Potylitsin, arXiv:cond-mat/9802279 v1 (1998).
9. A. F. Akkerman, M. Ya. Grudskii, and V. V. Smirnov, *Secondary Electron Emission from Solids under the Influence of Gamma Quanta* (Energoatomizdat, Moscow, 1986) [in Russian].
10. A. N. Aleinik, A. N. Baldin, E. A. Bogomazova, et al., Pis'ma Zh. Eksp. Teor. Fiz. **80**, 447 (2004) [JETP Lett. **80**, 393 (2004)].
11. W. H. McMaster, N. Kerr del Grande, J. H. Mallet, and J. H. Hubbell, Lawrence Radiation Laboratory, University of California, Livermore UCRL-50174, Sec. II. Rev. 1.
12. Y. Takabayshi, I. Endo, K. Ueda, et al., Nucl. Instrum. Methods Phys. Res. B **243**, 453 (2006).
13. B. G. Bacon and R. D. Lowde, Acta Crystallogr. **1**, 303 (1948).
14. D. A. Baklanov, I. E. Vnukov, Yu. V. Zhandarmov, et al., in *Proceedings of the 40th Intern. Conference on Physics of Interaction of Charged Particles with Crystals* (Universitetskaya kniga, Moscow, 2010), p. 86.
15. D. A. Baklanov, I. E. Vnukov, Yu. V. Zhandarmov, and R. A. Shatokhin, Poverkhnost', No. 4, 31 (2010) [J. Surf. Invest. **4**, 295 (2010)].